Cell, Vol. 118, 567–578, September 3, 2004, Copyright ©2004 by Cell Press

Vertebrate Shugoshin Links Sister Centromere Cohesion and Kinetochore Microtubule Stability in Mitosis

Adrian Salic,[1,*] Jennifer C. Waters,[1,2] and Timothy J. Mitchison[1]
[1]Department of Systems Biology
[2]Department of Cell Biology
Harvard Medical School
240 Longwood Avenue
Boston, Massachusetts 02115

Summary

Drosophila MEI-S332 **and fungal** ***Sgo1*** **genes are essential for sister centromere cohesion in meiosis I. We demonstrate that the related vertebrate Sgo localizes to kinetochores and is required to prevent premature sister centromere separation in mitosis, thus providing an explanation for the differential cohesion observed between the arms and the centromeres of mitotic sister chromatids. Sgo is degraded by the anaphase-promoting complex, allowing the separation of sister centromeres in anaphase. Intriguingly, we show that Sgo interacts strongly with microtubules in vitro and that it regulates kinetochore microtubule stability in vivo, consistent with a direct microtubule interaction. Sgo is thus critical for mitotic progression and chromosome segregation and provides an unexpected link between sister centromere cohesion and microtubule interactions at kinetochores.**

Introduction

Mitosis in eukaryotic cells is carefully monitored and controlled by checkpoint mechanisms that assay the kinetochore (Kt)-microtubule (MT) interaction to ensure proper chromosome segregation. In prometaphase, paired sister Kts must bind MTs from opposite spindle poles and eventually line up in bipolar orientation at the spindle's equator, forming the metaphase plate. If the Kt-MT interaction is abnormal, checkpoint pathways are activated (reviewed in Cleveland et al. [2003]), resulting in the inhibition of the anaphase-promoting complex (APC), a critical E3 ubiquitin ligase (Peters, 2002) required for the destruction of mitotic substrates, including cyclin and securin. There is evidence that checkpoint pathways monitor both binding of MTs to Kts and tension at Kts (Li and Nicklas, 1995), the latter being dependent on dynamic Kt-MT interactions.

Proper alignment of chromosomes and their segregation in mitosis also relies on cohesion between sister chromatids, although if and how Kt function and cohesion are integrated in mitosis is currently unknown. Sister cohesion requires cohesin, a multiprotein complex; one of its subunits, Scc1, must be proteolyzed by the cysteine protease separase (Uhlmann et al., 2000) in order to lose cohesion at anaphase onset. Separase also functions in meiosis to cleave Rec8, the meiosis-specific cohesin subunit homologous to Scc1 (Buonomo et al., 2000).

Cohesion between sister chromatids in vertebrates is lost in two steps. First, during prophase and prometaphase, the bulk of vertebrate Scc1 dissociates from chromosome arms following phosphoryation by polo kinase (Sumara et al., 2002). Chromatids separate completely at anaphase when vertebrate separase is activated and cleaves the remaining Scc1 at centromeres (Hauf et al., 2001). Drug treatments as well as timelapsed microscopy of mitotic cells suggest that chromatid separation along the arms and at the centromere are distinct processes (reviewed in Rieder and Cole [1999]). Perhaps the best illustration of differential cohesion occurs in meiosis. Cohesion along the arms of paired chromatids is lost in meiosis I but inter-Kt cohesion is maintained, a requirement for sister chromatid cosegregation. In meiosis II, inter-Kt cohesion is dissolved, allowing sister chromatid separation. Protection of intercentromeric cohesion in meiosis I requires *MEI-S332* in *Drosophila* (Kerrebrock et al., 1995; Moore et al., 1998) and *Sgo1* in yeast (Kitajima et al., 2004; Marston et al., 2004; Rabitsch et al., 2004; Katis et al., 2004). If MEI-S332 or Sgo1 is deleted, cohesion is lost prematurely in meiosis I; this correlates with a premature loss of Rec8 from sister centromeres in yeast. Interestingly, Sgo1 plays a role during mitosis in yeast; however, the underlying mechanism is still obscure and there is currently no agreement on whether Sgo1 is required for mitotic sister centromere cohesion (Kitajima et al., 2004; Marston et al., 2004; Katis et al., 2004).

It has not been clear if similar mechanisms regulate centromeric cohesion in metazoan mitosis, particularly in vertebrates. We have identified Sgo, a novel vertebrate Kt protein, based on its ability to stabilize MTs in *Xenopus* egg extracts. Vertebrate Sgo shows low sequence homology to both Sgo1 and MEI-S332 and is required for cohesion of mitotic sister Kts at metaphase. APC-mediated proteolysis degrades Sgo upon anaphase onset, allowing sister centromere separation. Unexpectedly but consistent with its MT-stabilizing activity in vitro, Sgo is required for Kt MT stability and MT-dependent tension at Kts during mitosis in vivo. We conclude that vertebrate Sgo plays a similar role in centromeric cohesion in mitosis as fly and yeast homologs perform in meiosis. Intriguingly, vertebrate Sgo also links cohesion of sister Kts and regulation of Kt-MT interactions, thus integrating two aspects critical for proper chromosome segregation in mitosis.

Results

Identification of *Xenopus* Sgo in a Microtubule Formation Assay

We devised an expression cloning strategy to identify factors that stimulate MT formation in mitotic *Xenopus* egg extracts. Briefly, small mRNA pools from a full-length normalized expression library (Carninci et al., 2000) were translated in fresh egg extracts containing

*Correspondence: adrian_salic@hms.harvard.edu

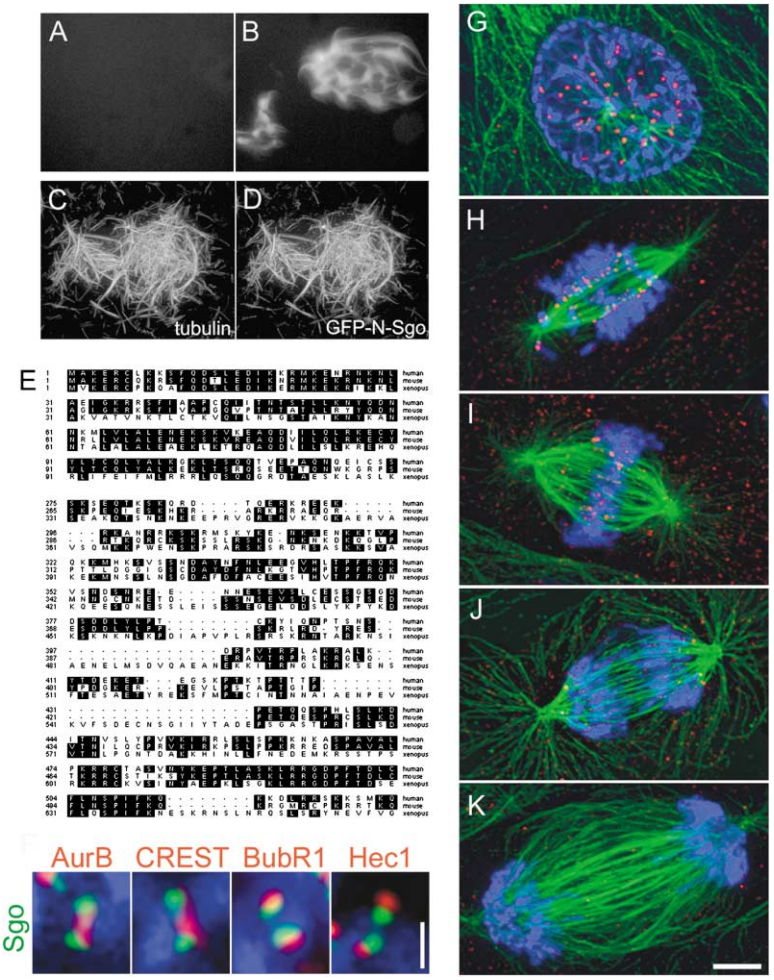

Figure 1. Identification of Sgo, a Novel Kinetochore Component that Can Bind Microtubules

(A and B) Expression cloning of *Xenopus* Sgo. mRNA pools from a normalized cDNA library were translated in fresh *Xenopus* egg extracts, in the presence of rhodamine-tubulin. (A) Inactive pool. (B) Pool containing *Xenopus* Sgo. Note that MTs became organized into aster-like structures in the mitotic extract.

(C and D) The N terminus of Sgo binds to and bundles MTs assembled from pure tubulin in vitro. GFP-N-mSgo (D) decorates rhodamine-labeled MTs (C).

(E) Sequence alignment of the N- and C-terminal conserved regions of human, murine, and *Xenopus* Sgo homologs.

(F) Magnified views of Kt pairs stained for myc-Sgo (green) and (left to right, in red/pink) AuroraB, CREST, BubR1, and Hec1. Chromosomes are in blue. The scale bar in (F) is 1 μm.

(G–K) Sgo (red/pink) localization in *Xenopus* mitotic cells. DNA is in blue and MTs are green. All images are maximum z projections of deconvolved spinning disk confocal optical sections collected every 0.3 μm through the entire spindle. Sgo is present on Kts in prophase (G), prometaphase (H), and metaphase (I). Note that Sgo staining decreases as Kts attach to the spindle. Sgo disappears from Kts in anaphase (J) and is virtually nondetectable in telophase (K). The scale bar in (K) is 5 μm.

fluorescent tubulin. Pools that caused the formation of MT structures were identified (Figures 1A and 1B) and the active clones were isolated. One clone thus isolated encoded a truncated importin α, consisting of the N-terminal importin β binding domain (not shown). This domain inhibits the interaction between importins α and β, thus stimulating the Ran pathway and releasing aster-forming activities (Gruss et al., 2001; Nachury et al., 2001). Identification of this truncated gene with its expected activity confirmed that our assay is suitable for identifying factors involved in MT formation.

A previously uncharacterized gene we identified was *Xenopus* Sgo. Three active pools contained *Xenopus* Sgo in our screen: two pools harbored full-length Sgo while one encoded a truncated Sgo gene, expressing only the N-terminal 170 amino acids of the protein. The latter was more potent in our assay than full-length Sgo, perhaps owing to higher expression levels and/or increased protein stability. By BLAST searching, we found Sgo homologs in other vertebrates; the homology between them clusters in two blocks—an N-terminal block predicted to form a coiled-coil and a C-terminal block rich in basic amino acids (Figure 1E). Aside from the coiled-coil and a number of putative nuclear localization sequences, Sgo does not contain any obvious domains or motifs. We were initially unable to identify Sgo homologs in invertebrate species. Human Sgo was recently proposed as a putative vertebrate homolog of fungal Sgo1 and Sgo2 (Kitajima et al., 2004; Rabitsch et al., 2004) and *Drosophila* MEI-S332 genes (Kerrebrock et al., 1995) involved in centromeric cohesion and chromosome segregation in meiosis.

Sgo Binds and Stabilizes Microtubules

XSgo was cloned by its ability to induce MT polymerization when overexpressed in *Xenopus* extracts (Figures 1A and 1B). Tagged XSgo expressed in extracts or in vitro translated XSgo supplied exogenously also cosediment with MTs in extracts (not shown). These results do not distinguish between a direct and an indirect interaction of Sgo with MTs since other factors in extracts might mediate MT polymerization enhancement and binding. Full-length recombinant Sgo was insoluble. Therefore, to determine if Sgo can bind MTs directly, we purified the GFP-tagged N-terminal fragment of mouse Sgo. In a visual assay, GFP-N-mSgo-decorated MTs assembled from purified tubulin in vitro, demonstrating that Sgo has MT binding potential (Figures 1C and 1D). Additionally, when the N-terminal fragment was attached to beads that were used to affinity purify binding proteins from *Xenopus* egg and HeLa cell extracts, the most abundant protein recovered was

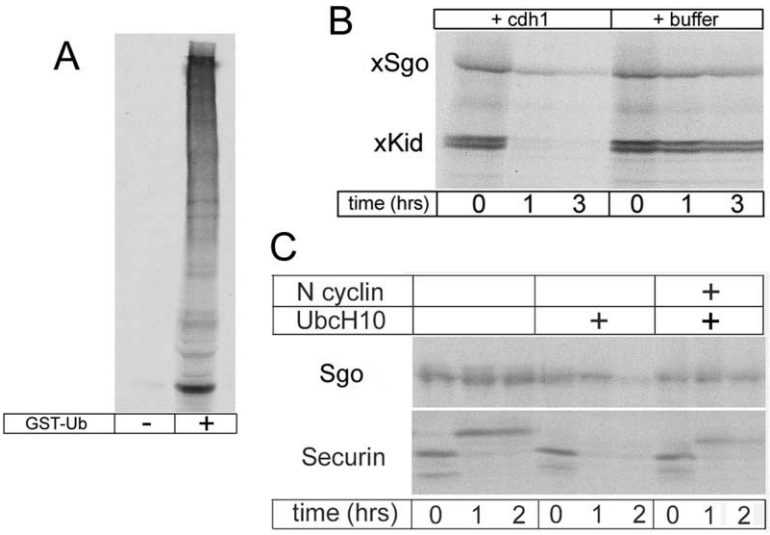

Figure 2. Sgo Is Degraded by the APC

(A) Radiolabeled XSgo is ubiquitinated in interphase *Xenopus* egg extracts supplemented with cdh1 and GST-ubiquitin. GST-ubiquitin conjugates were isolated on glutahione beads and XSgo conjugates were visualized by SDS-PAGE and autoradiography.

(B) The APC activator cdh1 accelerates XSgo degradation in interphase *Xenopus* egg extracts. XKid (Funabiki and Murray, 2000) was used as a control substrate of cdh1. Radiolabeled XSgo and XKid were added to extracts supplemented with cdh1 (+cdh1) or not (+buffer). The amount of protein remaining after the indicated times was detected by SDS-PAGE and autoradiography.

(C) Sgo and securin (positive control) are stable in mitotic extracts from nocodazole-arrested HeLa cells in which APC is inhibited by the spindle assembly checkpoint. Addition of UbcH10, an APC-specific E2 ubiquitin ligase, bypasses the checkpoint and rescues APC activity, overcoming the block to Sgo and Securin degradation. Degradation is efficiently competed by the N terminus of cyclin B, an APC substrate.

tubulin (not shown). Further demonstrating its ability to bind MTs assembled in vitro from pure tubulin, N-mSgo strongly bundles and stabilizes MTs against cold-induced depolymerization (Supplemental Figure S1 at http://www.cell.com/cgi/content/full/118/5/567/DC1).

Sgo Localizes to Kinetochores and Is Degraded by APC

In cultured cells, both tagged and endogenous Sgo localize to Kts in mitosis. In HeLa cells, tagged Sgo is found outside the domain staining for CREST (a centromeric stain) and AuroraB (an inner centromere protein), and inside the BubR1 and Hec1 domains (Figure 1F). These results suggest that Sgo localizes between the fibrous corona and the underlying centromeric chromatin, around the inner or outer Kt plate. MT plus ends are known to penetrate to around this depth (McEwen et al., 1998), consistent with potential Sgo-MT interactions.

We also examined the localization of endogenous Sgo during mitosis in cultured *Xenopus* cells (Figures 1G–1K). Sgo immunoreactivity at Kts is strong in prophase and prometaphase and weaker after the chromosomes attach to the spindle and align at the metaphase plate (Figures 1G–1I). Sgo staining disappears from Kts as cells undergo anaphase (Figure 1J). An identical staining pattern through mitosis is seen if Kt MTs are depolymerized before fixation (Supplemental Figure S2 on *Cell* website), demonstrating that the disappearance of Sgo staining in anaphase represents real loss of Sgo from Kts and not epitope masking by MTs. In meiotic spindles assembled in *Xenopus* egg extracts, Sgo also localizes to Kts in metaphase and disappears in anaphase (not shown).

In vitro translated Sgo is degraded in *Xenopus* extracts, likely by the ubiquitin-proteasome system, as ubiqutin conjugates of labeled Sgo are recovered when tagged ubiquitin is added to extracts (Figure 2A). The disappearance of Sgo from Kts at anaphase is reminiscent of APC substrates; additionally, vertebrate Sgo proteins contain several putative destruction boxes, motifs known to target proteins for APC-mediated destruction. Sgo degradation in *Xenopus* interphase extracts is stimulated by cdh1, an activator of APC (Figure 2B). To better define the degradation characteristics of Sgo, we turned to extracts from synchronized human somatic cells. As shown in Figure 2C, Sgo is not degraded in extracts from nocodazole-arrested HeLa cells (in which the spindle assembly checkpoint is active and Mad2 inhibits cdc20-APC). Recombinant UbcH10 restores the activity of cdc20-APC in extracts from nocodazole-arrested cells (M. Rape and M.W. Kirschner, personal communication). Addition of UbcH10 also rescues Sgo proteolysis in nocodazole extracts (Figure 2C); degradation of Sgo in these extracts is efficiently competed by the N terminus of cyclin B. This fragment of cyclin B contains a destruction box recognized by both cdc20- and cdh1-APC, further demonstrating that Sgo is a substrate for APC/C. Sgo is thus degraded by both cdc20- and cdh1-APC, explaining its disappearance from Kts during the metaphase to anaphase transition in cells.

Sequence analysis of vertebrate Sgo genes reveals several putative separase cleavage sites; however, neither mouse nor *Xenopus* Sgo were cleaved by purified active separase in vitro, suggesting that Sgo might not be a separase substrate (not shown).

Sgo Depletion Causes Mitotic Arrest with Loss of Sister Kinetochore Cohesion

We used RNA interference (RNAi) in HeLa cells to explore the function of Sgo in vivo. We confirmed by immunoblotting that our RNAi protocol caused an ~90% reduction in the amount of Sgo protein after 24 hr (Figure 3A). As this assay does not take into account siRNA transfection efficiency, we measured Sgo levels at Kts by microinjecting labeled antibodies into control cells or cells displaying the Sgo RNAi phenotype (see below). Measuring the fluorescence of individual Kt images collected with a CCD camera, we calculated a 13-fold de-

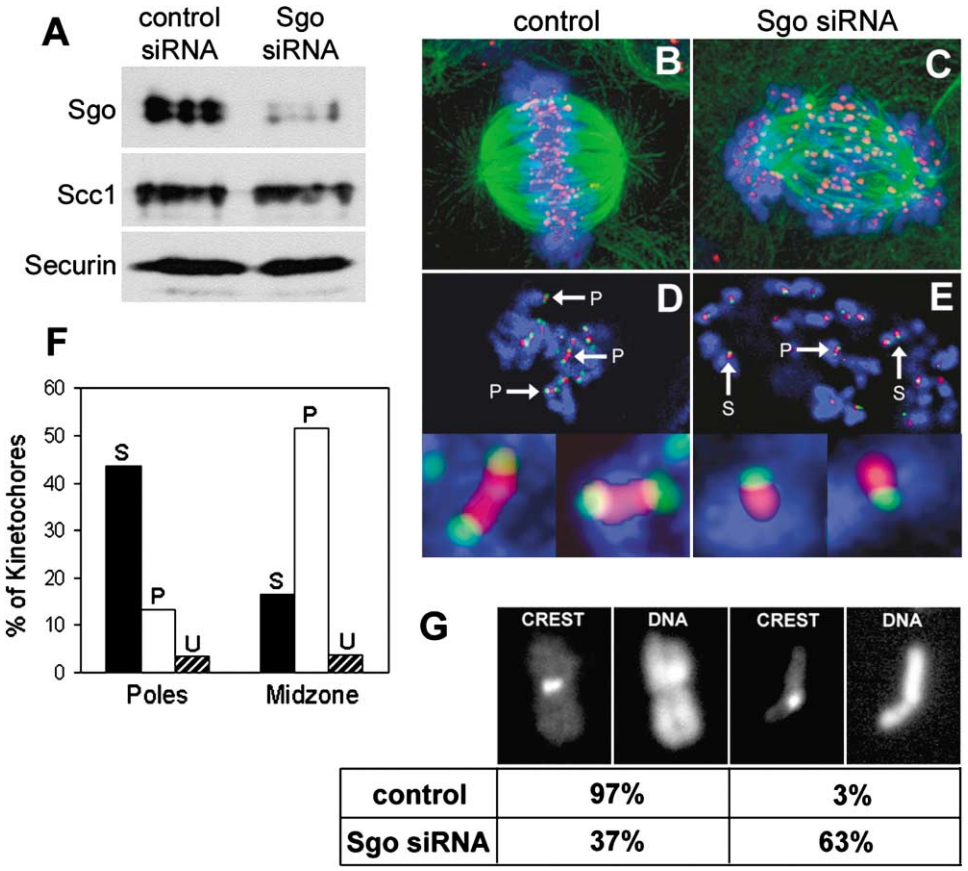

control	97%	3%
Sgo siRNA	37%	63%

Figure 3. Human Sgo RNAi Causes Mitotic Arrest with Loss of Sister Kinetochore Cohesion

(A) Western blot showing the efficiency of Sgo protein knockdown by RNAi. Control and SgosiRNA mitotic cells were collected by blow-off 24 hr after siRNA transfection. Sgo levels are decreased 90% while Scc1 and securin levels are not changed by RNAi.

(B and C) HeLa cells 18 hr after adding the control or the anti-Sgo siRNA, stained for DNA (blue), MTs (green), and Kts (pink/red, CREST staining). Maximum z projections of deconvolved spinning disk confocal optical sections were collected every 0.3 μm through the entire spindle. (B) Control cell in metaphase. Chromosomes are aligned and form a tight metaphase plate. (C) Sgo siRNA cell arrested in mitosis with unaligned chromosomes.

(D and E) Loss of centromeric cohesion following Sgo siRNA. Single optical sections chosen from a spinning disk confocal z series of HeLa cells stained for CREST (pink/red), Hec1 (green), and DNA (blue). (D) Control cell in prometaphase. Three paired (P) Kts are indicated by arrows and two are shown magnified in insets below. (E) SgosiRNA cell arrested with unpaired, single (S) Kts. The asterisks in (C) and (D) mark the spindle poles.

(F) Single Kts localize predominantly near the spindle poles in SgosiRNA cells. The middle third of the spindle is the midzone (where the metaphase plate would normally form) while the peripheral thirds contain the spindle pole regions. Six hundred and two Kts were counted in ten siRNA-treated cells. S = single, unpaired Kts, P = paired Kts, U = undetermined; Kts that could not be convincingly identified as single or paired.

(G) Chromosomes were isolated from control and SgosiRNA mitotic HeLa cells, stained for CREST and DNA. Percentage single and paired chromatids are shown.

crease in the average amount of Sgo at Kts following 24 hr RNAi treatment (Supplemental Figure S3 online).

RNAi of Sgo causes cells to arrest in mitosis 12–24 hr post-transfection; the mitotic index increases from 5% (control) to 25%–40% (SgosiRNA). In Sgo-depleted cells, chromosomes and their centromeres do not align to form a metaphase plate; instead, they are scattered throughout the cell (Figures 3B and 3C). The majority of SgosiRNA spindles appear normal, are bipolar, and display normal γ-tubulin staining at the poles (not shown) though an increased frequency of spindles with multiple poles was noted. We also observed an increase in spindle length in SgosiRNA cells (see below).

SgosiRNA cells are likely arrested in metaphase, due to the activation of the spindle assembly checkpoint. Consistent with this interpretation, the levels of securin are the same in SgosiRNA cells and nocodazole-arrested control cells (Figure 3A), indicating a block to APC activity. Additionally, the arrest caused by Sgo depletion is completely bypassed by overexpression of dominant-negative BubR1 (Taylor and McKeon, 1997) or chemical inhibition of AuroraB kinase (Ditchfield et al., 2003; Hauf et al., 2003), two treatments known to overcome checkpoint activation (not shown).

MEI-S332 in *Drosophila* and Sgo1 in yeast are required for meiotic sister centromere cohesion. To determine if vertebrate Sgo is necessary for mitotic centromere cohesion, we collected z series optical sections of Sgo-depleted cells stained for both CREST and Hec1 (an outer Kt corona marker). This method allowed us to

reliably distinguish paired from unpaired Kts in 3D images; paired Kts could be seen as green Hec1 dots flanking red CREST staining, while CREST staining associated with only one green Hec1 dot was categorized as single (i.e., unpaired). In mitotic SgosiRNA cells, there is a dramatic increase in the number of single Kts (59% of Kts were single, 33% paired, and 8% unknown; n = 602 Kts counted in 10 cells), indicating a loss of Kt cohesion (Figures 3D and 3E). In control mitotic cells, our measuring technique detected 95% of Kts as paired, 0% single, and 5% unknown (n = 308 Kts counted in 3 control cells). To ensure that the Kts that were counted as single in SgosiRNA cells were not actually paired Kts that were close enough to one another to be below the resolution limit of our microscope, we measured Hec1 fluorescence intensity of single and paired Kts in SgosiRNA cells. We found both average and integrated intensity values to be similar for single and paired Kts (not shown), confirming the correct identification of single Kts. Sgo inhibition by RNAi thus causes premature loss of Kt cohesion in mitosis with no effect on Hec1 levels per Kt. We also examined the spatial distribution of single Kts relative to the spindle (Figure 3F). Single Kts cluster in the spindle pole regions, while Kt pairs tend to occupy an equatorial position. This distribution is consistent with single Kts attaching to only one spindle pole and the absence of pulling forces from the opposite pole.

Finally, we examined sister chromatid pairing in chromosomes isolated by low salt/digitonin lysis and pelleting through a sucrose cushion from control (nocodazole-arrested) and SgosiRNA cells in mitosis. As shown in Figure 3G, Sgo RNAi resulted in a dramatic increase in the number of single chromatids (63% single, 37% paired after Sgo RNAi, n = 1398 single chromatids counted; compared to 3% single, 97% paired in control mitotic cells, n = 1850 single chromatids counted).

Multiple Roles of Sgo in Mitosis: Evidence from Live Imaging of Cohesion Loss after Sgo Depletion

After establishing that Sgo is required for sister Kt cohesion, we next investigated the timing of premature sister Kt separation in mitosis after Sgo RNAi. By long-term imaging of histone2B-GFP-expressing HeLa cells, we observed two distinct behaviors of mitotic SgosiRNA cells, depending on the time elapsed from siRNA transfection, presumably reflecting progressively decreased Sgo levels with time.

Early in the course of RNAi (12–20 hr post-transfection), affected cells entered mitosis and formed what appeared to be a normal metaphase plate (average time from prophase to a tight metaphase plate = 32 min, n = 40 cells compared to 30 min in controls, n = 39), indicating that chromosome congression was normal. However, these cells became arrested in mitosis, and after an average of 87 min (n = 40 cells), chromosomes began to leave the metaphase plate and move toward the spindle poles (Figure 4A and Supplemental Movie S1 on *Cell* website), reflecting premature disjunction and segregation. The phenotype gradually became more severe, as more chromatids left the plate and moved polewards. In contrast, control cells took an average of 39 min to progress from metaphase to mid-anaphase (n = 39 cells).

Later in the course of RNAi (20–30 hr post-transfection), affected cells entered mitosis but did not attempt to align their chromosomes, which remained completely scattered suggesting loss of cohesion at the onset of mitosis or earlier (Figure 4B and Supplemental Movie S2 online).

To better define the loss of sister chromatid cohesion seen early after RNAi, we performed 4D imaging of HeLa cells expressing GFP-CENP-A. Figure 4C (and Supplemental Movie S3) shows normal mitotic progression in these cells. When Sgo is partially knocked down (Figure 4D and Supplemental Movie S4), paired centromeres first align properly at the metaphase plate, with timing indistinguishable from control cells. Instead of initiating anaphase, single centromeres in SgosiRNA cells begin to dissociate and move poleward following a period of metaphase arrest.

We conclude that low levels of Sgo provide sufficient cohesion to allow chromosome congression in SgosiRNA cells but another aspect of Sgo function is perturbed, such as MT dynamics, accounting for checkpoint activation and mitotic arrest followed by eventual loss of cohesion.

Sgo Is Required for Tension at Kinetochores and Normal Kinetochore Structure

We examined if Sgo has a role in Kt function and structure. A significant number of Kts in SgosiRNA cells are still paired; we next asked if these paired Kts behaved normally. Proper bipolar attachment of Kts to the spindle results in MT-dependent tension between paired Kts. We estimated tension at Kts (Waters et al., 1996) in SgosiRNA cells by measuring the distance between paired Kts at metaphase in HeLa cells stained for CREST and Hec1 (Figures 5A and 5B). The distance between Hec1 staining of sister Kts in SgosiRNA cells is significantly decreased (average of 0.9 μm, range 0.5–1.7 μm, n = 151 Kt pairs in 6 cells) compared to controls (average 1.4 μm, range 0.8–2.1 μm, n = 117 Kt pairs in 3 cells), indicating a loss of tension at Kts following Sgo depletion. In live HeLa cells expressing GFP-tagged human Mis12, the distance between sister Kts in SgosiRNA cells is dramatically decreased (average of 0.52 μm, n = 53 Kt pairs) compared to controls (average 0.93 μm, n = 134 Kt pairs). Mechanically, tension at Kts has the effect of pulling the spindle poles toward each other. Thus another measure for tension at Kts is the overall length of the spindle (DeLuca et al., 2002). Consistent with a reduction in tension at Kts, spindle length increases from an average of 8.1 μm (range 5.9 to 10.2 μm, n = 10 cells) in control metaphase HeLa cells to an average of 15.1 μm (range 10.7 to 21.2 μm, n = 19 cells) in SgosiRNA HeLa cells.

Reduced tension at Kts can be caused by either loss of MTs bound to Kts or inhibition of Kt MT dynamics. To visualize Kt MT bundles, we depolymerized non-Kt MTs by calcium treatment. In control metaphase cells, each Kt pair contacts two corresponding bundles of MTs, one from each spindle pole. In Sgo-depleted cells, bundles of MTs were seen bound to the majority of Kts, both those near the poles and those at the equator of

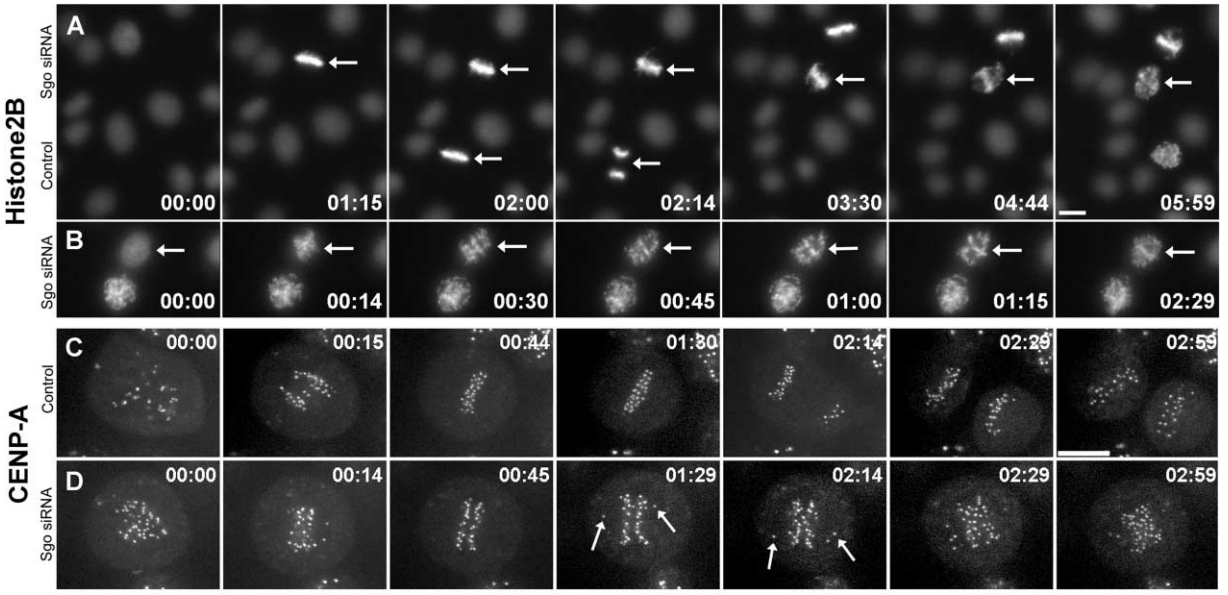

Figure 4. Live Imaging of Cohesion Loss after Sgo RNAi

(A) Widefield fluorescence images from a timelapse of HeLa cells expressing histone2B-GFP, 12–18 hr after Sgo siRNA transfection. Top arrow points to an SgosiRNA cell. Note that chromosome congression to the metaphase plate is normal yet the cell arrests in mitosis. After approximately 60 min, chromatids are seen detaching from the plate and move poleward. The bottom arrow points to an unaffected cell undergoing mitosis. The calibration bar is 10 μm. Elapsed time is shown as hh:mm.

(B) Twenty-four to thirty hours after RNAi cells were imaged as in (A). The cell marked by the arrow enters mitosis but chromosomes remain scattered and do not attempt to congress.

(C) Maximum z projections from a 4D spinning disk timelapse showing normal mitosis in a control HeLa cell expressing GFP-CENP-A. The calibration bar is 5 μm.

(D) SgosiRNA HeLa cell imaged as in (C), 18 hr after RNAi. At 45 min from prophase, paired centromeres align at the metaphase plate. Within 45 min, unpaired centromeres (two of them marked by arrows) dissociate from the plate and move poleward.

the spindle (Figures 5C and 5D). Since KT MTs are present and attached to Kts by this assay, it is likely that tension is reduced due to an effect on Kt MT dynamics (see below), as has been shown in taxol-treated cells where tension is lost though Kts still bind MTs (Waters et al., 1999).

We examined how loss of Sgo affects components of the various subdomains of the centromere-Kt complex. CREST (Figures 3B and 3C) and AuroraB (Figures 5E and 5I) staining are normal in Sgo-depleted cells, suggesting that loss of Sgo does not disrupt the structure of the centromere and inner centromere, respectively. BubR1 (Figures 5F and 5J) staining is also normal in SgosiRNA cells. In contrast, CENP-E (Yao et al., 2000) (Figures 5G and 5K) and CENP-F (Rattner et al., 1993) (Figures 5H and 5L), two outer Kt components, are reduced 2.9- and 2.3-fold, respectively. Interestingly, Hec1, an outer Kt component required for Kt-MT interaction (DeLuca et al., 2002; Martin-Lluesma et al., 2002; McCleland et al., 2003), is largely unperturbed by Sgo depletion (Figures 5A and 5B). We conclude that a subset of Kt components depends on Sgo for their localization.

Sgo Depletion Destabilizes Kinetochore Microtubules

As Sgo contains a potent MT binding domain, we tested if alterations in MT dynamics might explain metaphase arrest of SgosiRNA cells in mitosis. Chromosomes aligned at the metaphase plate normally display oscillatory movements along the spindle axis. These oscillations occur as Kt MTs switch between states of growth and shortening (Skibbens et al., 1993). We first imaged the effect of SgosiRNA on chromosome oscillations in HeLa cells expressing histone2B-GFP. We observed chromosome oscillations in both SgosiRNA cells (Figure 6B and Supplemental Movie S6 online) and control mitotic cells (Figure 6A and Supplemental Movie S5).

To assay MT dynamics directly, Sgo was knocked down by siRNA in HeLa cells expressing α-tubulin tagged with photoactivatable (PA) GFP (Patterson and Lippincott-Schwartz, 2002). We then photoactivated PA-GFP in a bar-shaped region approximately perpendicular to the long axis of the mitotic spindle; the photoactivation was followed by timelapsed imaging of the fluorescent marks thus formed on Kt MTs (Mitchison, 1989). When photoactivation is performed on spindles, Kt MTs, non-Kt MTs, and free tubulin in the activated region become fluorescent. But because the turnover of non-Kt MTs is very fast and free tubulin diffuses quickly from the photoactivation site, within seconds the most prominent photoactivation marks left on the spindle are on the more stable Kt MTs. This method is thus well suited to image Kt MT dynamics. In control cells, the fluorescent marks on Kt MTs lose fluorescence slowly and move poleward on the spindle (Figures 6C–6E) at a rate of 0.5 μm/min, consistent with published

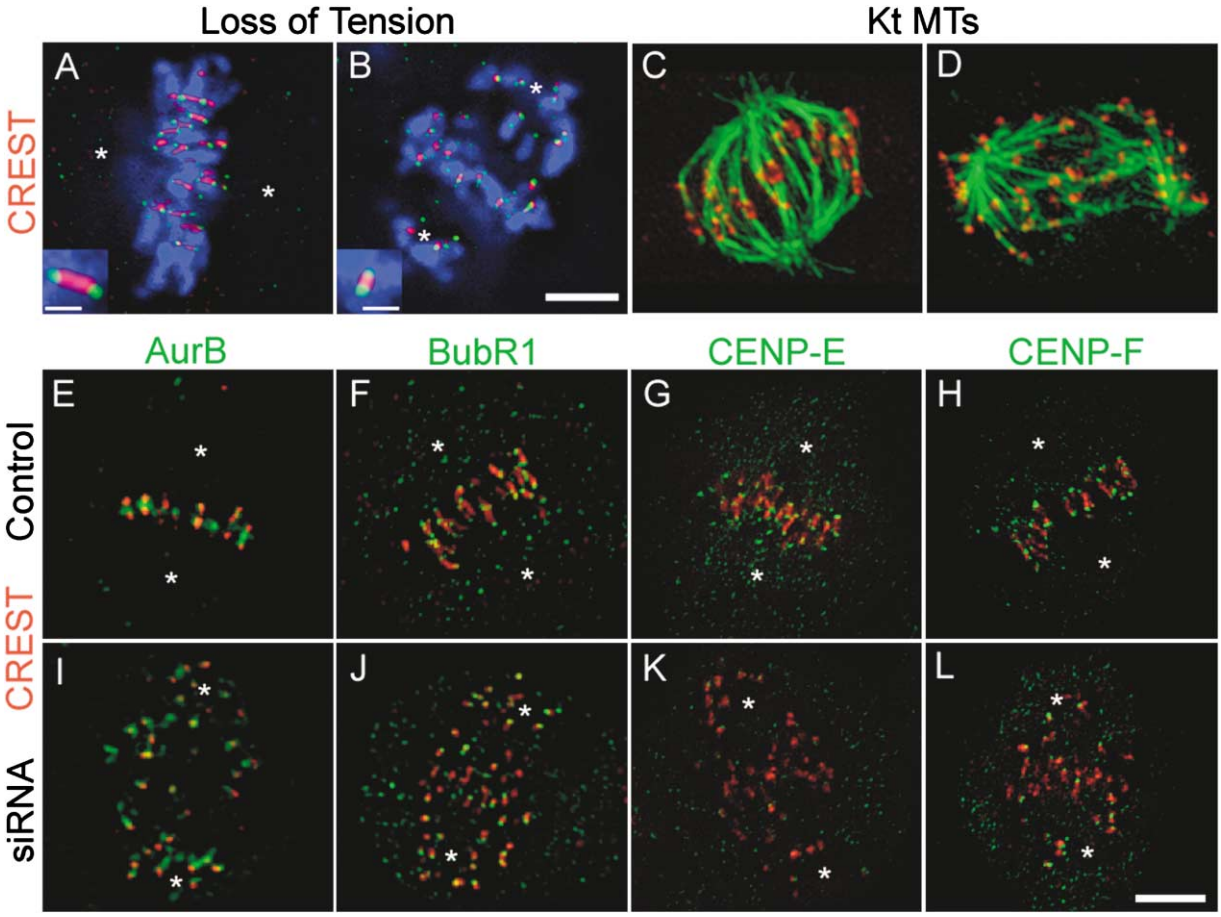

Figure 5. Effect of Sgo Depletion on Tension at Kinetochores, K Fibers, and Other Kinetochore Components

(A and B) Loss of tension at Kts in arrested cells 24 hr after Sgo depletion. Single optical sections from spinning disk confocal z series of HeLa cells stained for CREST (pink/red), Hec1 (green), and DNA (blue). (A) Control and (B) SgosiRNA cells, respectively. Single Kt pairs are shown in insets (bar = 1 μm); the positions of the spindle poles are marked with asterisks. Note the decrease in the inter-Kt distance for Kts that are still paired in SgosiRNA cells. The bar in (B) is 5 μm.

(C and D) Kt MTs are still present after Sgo RNAi. Control and SgosiRNA HeLa cells were permeabilized, treated with calcium to depolymerize non-Kt MTs, fixed, and stained for CREST (red) and tubulin (green). Images are z projections of confocal optical sections collected every 0.3 μm through the entire spindle. (C) Control cell in metaphase. (D) SgosiRNA cell arrested in mitosis.

(E–L) Effect of Sgo depletion on various Kt components. Images are z projections of 3–4 sequential confocal optical sections collected every 0.3 μm. Control and Sgo siRNA-treated HeLa cells were stained red for CREST, blue for DNA, and green for AuroraB (E and I), BubR1 (F and J), CENP-E (G and K), and CENP-F (H and L). The scale bar in (L) is 5 μm. The asterisks in (E)–(L) mark the approximate position of the spindle poles.

values for Kt MT dynamics in vertebrate somatic cells (Zhai et al., 1995; Waters et al., 1996). In SgosiRNA cells, the fluorescent bar dissipates rapidly, indicating a dramatic decrease in Kt MT stability (Figures 6F–6H). To quantitate this effect, we measured the decrease in the intensity of the fluorescent bar (relative to the total GFP fluorescence in the spindle, to control for photobleaching) over time as a measure of Kt MT turnover. In control HeLa cells, the intensity of the bar decreases on average from 100% to 59% in 3 min (n = 7 cells) while in SgosiRNA cells, the average change is from 100% to 18% in 2 min (n = 27 cells, Figure 6I). It was difficult to detect poleward flux in SgosiRNA cells due to the fast turnover of Kt MTs. The kinetics are not truly exponential but we estimate that Kt MT half-life is decreased at least 3-fold by Sgo RNAi, demonstrating that Sgo plays a critical role in regulating the stability of Kt MTs in mitosis.

Sgo Function in Mitosis: Evidence from Anti-Sgo Antibody Injections

The SgosiRNA phenotype indicated that Sgo is required for sister chromatid cohesion and Kt MT dynamics but did not give us an indication of the timing for the Sgo requirement during the cell cycle. Sgo might be required during mitosis; alternatively, its function might be required in interphase during Kt assembly. We addressed this question by microinjection of affinity-purified anti-Sgo antibodies into cultured *Xenopus* cells in early prometaphase. This experiment is different from a loss-of-function SgosiRNA, as the antibody might block the interaction of Sgo with MTs, Sgo proteolysis, and/or might even activate some function of Sgo by "opening" the protein. The fluorescently labeled antibodies localized to Kts within minutes following microinjection, thus confirming that they were capable of binding their target

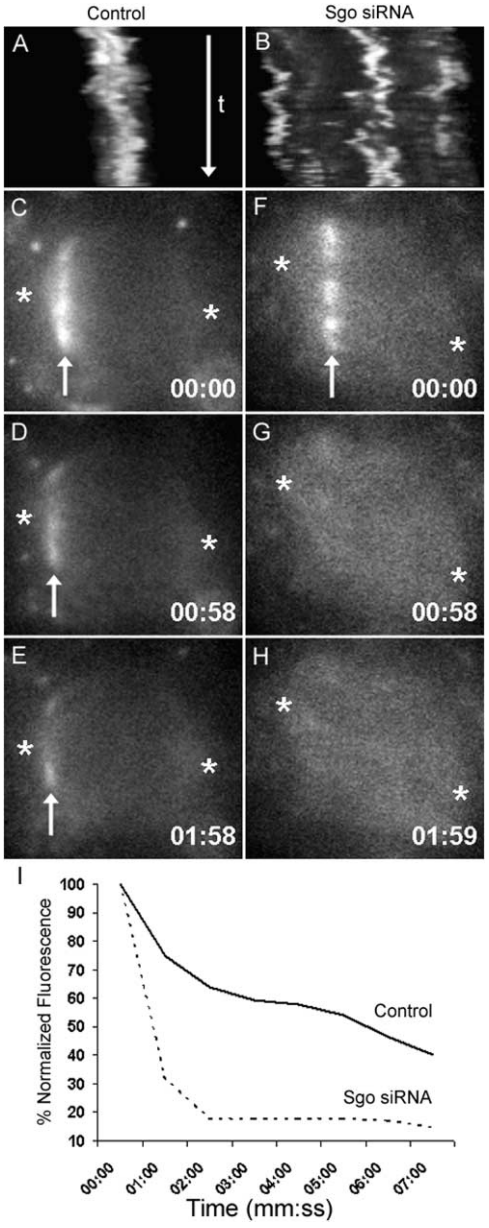

Figure 6. Effect of Sgo Depletion on Kinetochore Microtubule Dynamics

(A and B) Kymographs showing chromosome oscillations perpendicular to the metaphase plate in control (A) or SgosiRNA (B) HeLa cells expressing histone2B-GFP. The kymographs represent 43.5 min timelapses, with one frame recorded every 30 s. Note oscillations of both the chromosomes of the metaphase plate and the chromosomes at the spindle poles in (B).

(C–E) Three frames from a timelapse of a control mitotic HeLa cell expressing PA-GFP-tubulin in which GFP fluorescence was activated in a bar-shaped region (indicated by the arrow) perpendicular to the spindle. Note the poleward movement of the bar.

(F–H) Three frames from a timelapse following photoactivation of a SgosiRNA cell. Note the rapid disappearance of the fluorescent bar. In (C)–(H), the approximate positions of the spindle poles are marked by asterisks.

(I) Graph showing the decrease in the relative intensity of the fluorescent bars. The control curve represents the average of 7 cells while 24 cells were averaged for the Sgo siRNA curve.

in live cells. Injection of prometaphase cells stopped or significantly delayed mitotic progression and anaphase onset (see Table 1).

We injected anti-Sgo antibodies into prometaphase *Xenopus* cells expressing GFP-CENP-A followed by live imaging of the fluorescent centromeres. Anti-Sgo antibody injections dramatically stopped chromosome oscillations (see kymographs in Figures 7A and 7B and Supplemental Movies S7 and S8), consistent with a role for Sgo in Kt-MT dynamics. Anti-Sgo injections in these cells often inhibited chromosome alignment at the metaphase plate and resulted in a 26% decrease in the inter-Kt distance from an average of 1.38 μm ($\pm$0.32 μm) in controls (213 Kts measured in 5 cells, range 0.68–2.76μm) to 1.02 μm ($\pm$0.23 μm) in anti-Sgo-injected cells (252 Kts measured in 5 cells, range 0.56–1.97 μm).

We measured the effect of anti-Sgo antibodies on Kt MT dynamics by microinjection into *Xenopus* mitotic cells expressing PA-GFP-tubulin, followed by localized photoactivation and timelapse. In control cells, the fluorescent marks on Kt MTs moved poleward on the spindle (Figures 7C–7E). In contrast, the fluorescent marks on Kt MTs of cells injected with anti-Sgo antibodies were stationary and no detectable poleward movement was observed (Figures 7F–7H). As shown in the graph in Figure 7I, in control cells the relative intensity of the bar decreases on average from 100% to 52% in 3 min (n = 6 cells) while in anti-Sgo-injected cells the average change is from 100% to 84% in 6 min (n = 4 cells). These results demonstrate that anti-Sgo antibodies block chromosome oscillation, stabilize Kt MTs, and also appear to block poleward flux.

Although anti-Sgo injection causes pronounced mitotic arrest, some injected cells undergo a delayed anaphase. We were unable to reliably detect a change in the rate of poleward chromosome movement in anaphase A in these cells. To follow individual Kts through the delayed anaphase, we imaged cells microinjected with fluorochrome-tagged anti-Sgo antibodies. We found that in many instances both Kts in a pair migrate to the same pole in anaphase (Figures 7J and 7K), suggesting that binding of the antibody to Sgo can block the dissolution of sister cohesion at anaphase. Kt localization of the labeled antibody was similar at metaphase and anaphase, in contrast to the disappearance of Sgo from Kts during normal anaphase. A likely explanation is that the antibodies block or delay degradation of Sgo. We confirmed in both *Xenopus* egg and somatic cell extracts that the anti-Sgo antibodies specifically block APC-dependent degradation of Sgo (Figures 7L and 7M). We thus conclude that inhibition of Sgo degradation by anti-Sgo antibodies can lead to sister chromatid nondisjunction and missegregation in anaphase.

Discussion

During meiosis I, cohesion between sister chromatids is lost along arms but protected between centromeres; this physical link at centromeres ensures that sisters cosegregate. Intercentromeric cohesion is finally lost in meiosis II and sisters separate. *MEI-S332* in *Drosophila* (Kerrebrock et al., 1995) and *Sgo1* in yeast (Kitajima et al., 2004; Marston et al., 2004; Rabitsch et al., 2004) are

Table 1. Summary of Anti-Sgo Antibody Injections into *Xenopus* XTC Cells

	Controls: Prometaphase to Anaphase Onset (n = 8)	Injected: Prometaphase to Anaphase Onset (n = 18 of 42)	Injected: Prometaphase to Cytokinesis/Blebbing (n = 24 of 42)
Average	00:19:58	00:47:26	01:38:25
Min	00:11:53	00:25:20	00:27:16
Max	00:25:20	01:48:10	05:48:03

Experimental and control cells were imaged by DIC or phase contrast. Anti-Sgo-injected *Xenopus* XTC cells either underwent delayed anaphase (middle column; see Figure 5 for an example of such a cell) or arrested for a while and then exited mitosis but their anaphase chromosome movements were difficult to assess by DIC. For the latter cells, we measured the time interval from prometaphase to cytokinesis. Time is shown as hh:mm:ss.

required to protect cohesion at centromeres in meiosis I. Although differential cohesion between arms and centromeres is known to occur in vertebrate mitosis also, the basis for it has remained obscure. In the present study, we identified vertebrate Sgo and showed that it is required to prevent premature loss of cohesion between centromeres in mitosis. This demonstrates that conserved mechanisms are employed in both meiosis and mitosis, as well as across phyla, to accomplish differential cohesion along paired sister chromatids.

How do sister centromeres connect at metaphase and what is the role of Sgo in this process? In yeast, Sgo1 is thought to protect Rec8 from separase in meiosis I and, by analogy, Sgo might protect centromeric Scc1 from separase in vertebrate mitosis. In the simplest model, Sgo binds the cohesin complex, predicting colocalization of Sgo and cohesin in the metaphase centromere. Sgo is localized underneath Kts, further out than inner centromere markers and further in than outer plate and corona markers. We do not currently know the exact relative location of Scc1 and Sgo in metaphase. Complicating this picture, we do not know exactly where sister DNA duplexes connect in the centromere. In our view, it is not clear that cohesin alone is responsible for centromeric cohesion in vertebrate metaphase; it is possible that part of this function is passed to another protein (such as Sgo) or even DNA topology (such as catenation or Holliday junctions) during prophase, when much of

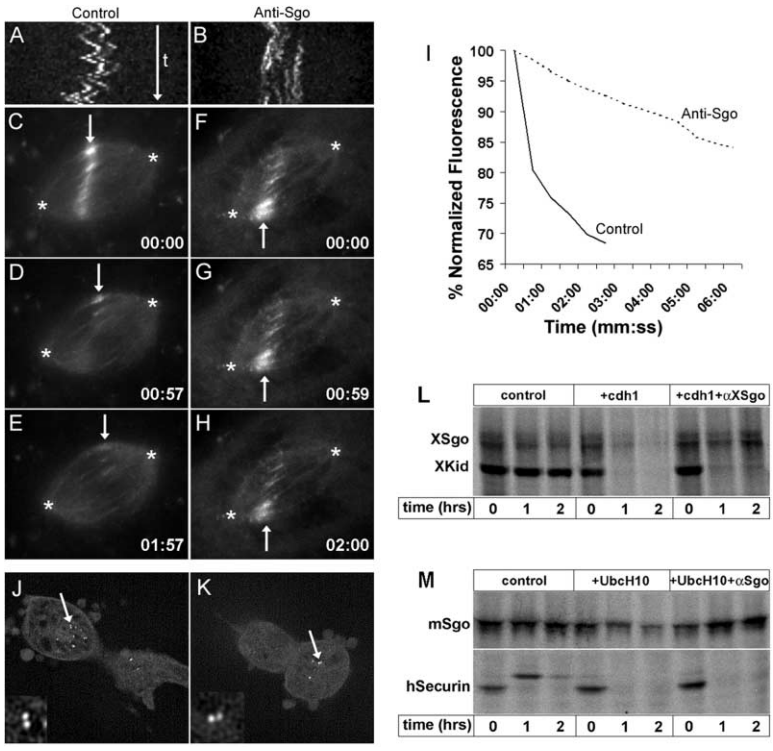

Figure 7. Anti-Sgo Antibody Injections Inhibit the Dynamics of Kinetochore Microtubules and Can Cause Chromosome Missegregation

(A and B) Kymographs showing chromosome oscillations in *Xenopus* XLK cells expressing GFP-CENP-A. (A) Control cell. (B) Cell microinjected with anti-XSgo antibodies just prior to the beginning of the timelapse. The kymographs represent 10 min movies, with one frame recorded every 15 s.

(C–H) Mitotic *Xenopus* XTC cells expressing PA-GFP-tubulin were injected with Alexa568-labeled anti-XSgo antibodies. GFP fluorescence was activated in a bar-shaped region perpendicular to the spindle and was imaged by timelapsed widefield fluorescence. (C–E) Three frames of a movie showing tubulin dynamics in a control mitotic cell. Shortly after activation, the fluorescent bar (marked by an arrow) decreases in intensity, as tubulin in non-Kt MTs turns over very quickly. What remains of the bar represents the more stable Kt MTs. Note the movement of the bar toward the two spindle poles, marked by asterisks. (F–H) Anti-Sgo antibody-injected cell. Note that the bar is stationary, indicating an inhibition of Kt MT dynamics. Time is shown as mm:ss.

(I) Graph showing the decrease in intensity of the fluorescent bars.

(J and K) Alexa488-labeled anti-Sgo antibodies were injected into prometaphase *Xenopus* XTC cells, some of which initiated a delayed anaphase. The Sgo-labeled Kts in these cells were optically sectioned live on a spinning disk confocal microscope. Individual focal planes from the Z stack are shown. The arrows point to some of the Kt pairs (shown magnified in the lower left corners of each frame) that did not separate during anaphase.

(L and M) Affinity-purified anti-Sgo antibodies specifically block the APC-dependent Sgo degradation. (L) Both XSgo and XKid are rapidly degraded by cdh1-APC in *Xenopus* egg extracts; addition of anti-XSgo antibodies blocks XSgo but not XKid degradation. (M) Anti-mSgo antibodies block mSgo but not hsecurin degradation in extracts from nocodazole-arrested HeLa cells supplemented with UbcH10. See also legend of Figures 2B and 2C for details.

the cohesin is removed from chromosomes. Interestingly, in Scc1-deficient vertebrate cells (Vagnarelli et al., 2004), sister chromatid association is not completely abolished. Discovery of Sgo should help elucidate the mechanism of sister chromatid cohesion in vertebrate metaphase.

One of the most intriguing and unexpected aspects of vertebrate Sgo is its potential for MT interaction, conferred by a potent MT binding and stabilizing domain in the N terminus. Vertebrate Sgo, however, is not detected along the length of MTs in vivo; therefore, if the MT stabilization phenotype exists in cells, it should be localized to the Kt MTs. Indeed, RNAi of Sgo strongly destabilizes Kt MTs while anti-Sgo antibody injection causes a dramatic stabilization of Kt fibers, indicating an abnormal Kt-MT interaction. We do not yet know if the antibody effect is a gain- or loss-of-function phenotype. Antibody injection stabilizes Sgo and causes some sister Kts to cosegregate (the opposite effect of RNAi depletion), suggesting gain of function is a likely possibility. In that case, the observed Kt MT stabilization might be mediated by direct interaction between Kt MTs and the MT-stabilizing domain of Sgo itself. Alternatively, the antibody effect may be indirect, causing loss of MT-destabilizing factors, such as AuroraB and MCAK (both implicated in destabilizing Kt MTs), from the Kt. Addressing these questions will require separation of Sgo function by mutagenesis in conjunction with in vitro biochemical assays of the Kt-MT interaction. Analyzing MT capture by purified Sgo-depleted chromosomes (Figure 3G) may also be useful. Additionally, it will be important to determine if yeast Sgo and *Drosophila* MEI-S332 also interact with MTs and if they regulate MT dynamics in a manner similar to vertebrate Sgo. Interestingly, Sgo2-GFP localizes to spindles in fission yeast, consistent with a possible MT interaction (Rabitsch et al., 2004).

Cohesion between centromeres is lost in anaphase, when APC degrades securin, and separase becomes active. We showed that Sgo is also a substrate of APC; thus both separase and its substrate Scc1 are regulated by inhibitors degraded by APC. It is also interesting that Sgo depletion by RNAi causes loss of CENP-E and CENP-F but not Hec1 from Kts. It is possible that this represents an effect on Kt assembly; alternatively, Sgo may regulate targeting of CENP-E and CENP–F to Kts. When Sgo is proteolyzed in anaphase, CENP-E and CENP–F (but not Hec1) disappear from Kts as well. We speculate that Sgo proteolysis and severing of inter-Kt contact are part of the upstream signal for maturation of Kts from a metaphase to an anaphase state; this hypothesis could be tested using a proteolysis-resistant Sgo mutant.

Sgo depletion causes human cells to arrest in mitosis, even if their chromosomes initially congress to form a normal metaphase plate; this is likely due to a loss of tension at Kts. Is Sgo required for tension generation by maintaining inter-Kt cohesion or does it play a more direct role? How does lack of Sgo activate the spindle assembly checkpoint? Is Sgo part of the elusive mechanism for sensing tension at Kts? Future experiments will need to address these important questions, starting with an analysis of Mad1/Mad2 at Kts in both Sgo-depleted and anti-Sgo-injected cells.

In summary, we propose that Sgo is required for proper mitotic progression and chromosome segregation and plays a dual role upstream and downstream of the spindle assembly checkpoint. On one hand, Sgo is required to hold sister Kts together until its destruction by APC/C and subsequent cleavage of Scc1 by separase. The spindle assembly checkpoint controls the activity of APC/C, ensuring that Sgo will be degraded only if Kts are properly attached to the spindle. On the other hand, through its regulation of MTs, Sgo influences the spindle assembly checkpoint. Sgo is thus a critical link between inter-Kt cohesion and Kt-MT interaction, bringing them both under the control of APC/C. Finally, it is worth noting that human Sgo (under the name NY-BR-85, a serologically defined breast cancer antigen) has been identified as a gene overexpressed 3- to 11-fold over normal in 90% of human breast cancers (Scanlan et al., 2001). This finding raises the important possibility that Sgo plays a role in carcinogenesis, perhaps by affecting the fidelity of chromosome segregation and thus contributing to chromosome instability and tumor aneuploidy.

Experimental Procedures

Expression Cloning of *Xenopus* Sgo

A full-length, normalized library was built from *Xenopus* egg mRNA (Carninci et al., 2000). mRNA pools representing 32 clones were translated in fresh egg extracts supplemented with rhodamine-tubulin. Pools that reproducibly caused the formation of MT structures were identified and further subdivided until single active clones were isolated.

Plasmids and Antibodies

N-mSgo, the N-terminal MT binding domain of mouse Sgo (171 amino acids starting at the N terminus), was expressed and purified from bacteria as a 6His-tagged eGFP fusion. Rabbit polyclonal antibodies were raised against maltose binding protein fusions of full-length *Xenopus* and mouse Sgo (MBP-XSgo and MBP-mSgo). Antibodies were affinity purified against antigen and fluorescently labeled with Alexa488 or Alexa568 NHS esters.

Microtubule Binding

MTs were polymerized in vitro from pure tubulin supplemented with X-rhodamine-labeled tubulin. MTs (30 μM) were mixed with GFP-N-mSgo (5 μM), incubated 10 min at 37°C, and fixed.

Microinjection into Cultured Cells, Imaging, and Photoactivation Experiments

Microinjection was done using an Eppendorf Injectman microinjector mounted on an inverted Nikon TE2000E microscope. Spinning disk confocal z series optical sections of fixed cells were collected using a Nikon TE2000U inverted microscope equipped with a Yokogawa spinning disk confocal and then deconvolved using AutoQuant software.

Live imaging of cells was done by timelapsed wide-field or spinning disk confocal fluorescence microscopy. Long-term 4D imaging of control and SgosiRNA HeLa cells expressing GFP-CENP-A was done on a spinning disk microscope, collecting a z series every 15 min. For each time point, six focal planes were collected using a 1 μm step size. For photoactivation experiments, we used HeLa or XTC cells expressing photoactivatable GFP (Patterson and Lippincott-Schwartz, 2002) fused to α-tubulin. For localized photoactivation, we placed a 25 μm $\times$ 3 mm slit in the field diaphragm plane of a Nikon TE2000E microscope to generate a 1–2 μm wide bar-shaped region on the specimen, as described (Mitchison, 1989). The fluorescent bar was then imaged by timelapsed 4D widefield fluorescence microscopy. The intensities of the fluorescent bar and of the entire spindle were measured over time. The ratio ([bar fluores-

cence/total fluorescence] t = x)/ ([bar fluorescence/total fluorescence] t = 0) × 100 was plotted against time.

Kymographs of chromosome oscillations in histone2B-GFP HeLa cells and GFP-CENP-A XLK cells were generated using the MetaMorph software.

Degradation and Ubiquitination Assays

Degradation reactions in *Xenopus* extracts were performed essentially as described (Salic et al., 2000). His-tagged human cdh1 (purified from baculovirus-infected Sf9 cells) was added to extracts to 20 μg/ml. Degradation reactions in HeLa extracts were performed using a protocol essentially identical to the one for egg extracts. For antibody blocking experiments, affinity-purified anti-XSgo or anti–mSgo antibodies were added to extracts to 100 μg/ml.

SiRNA Experiments

RNAi of HeLa cells was performed as described (Elbashir et al., 2001). The active siRNA duplex used in the experiments presented in this paper targeted the following sequence of the human Sgo mRNA: 5′AAGATATCATCCTACAGCTGA 3′.

To determine the number of single Kts, HeLa cells were stained for both CREST and Hec1, and z series were collected on a spinning disk confocal. Single Kts were differentiated from paired Kts by the presence of single juxtaposed dots of CREST and Hec1 staining. Measurement of inter-Kt distances was also done on fixed HeLa cells stained for CREST and Hec1.

To assay the effect of Sgo knockdown on various Kt components, spinning disk confocal images of HeLa cells were collected every 0.3 μm through the entire spindle, using identical camera acquisition settings for each given immunostained protein. Labeled kinetochores were selected using grayscale value thresholding, and integrated intensity values were recorded. The ratio of individual kinetochore proteins to CREST values were compared between control and Sgo siRNA cells. Five to six cells were analyzed for each experimental condition.

Chromosomes were purified from control siRNA cells arrested in mitosis by nocodazole treatment and from HeLa cells arrested in mitosis by Sgo siRNA, spun onto poly-lysine-coated coverslips, stained for CREST and DNA, and scored visually for sister chromatid pairing.

Acknowledgments

We thank the Nikon Imaging Center at Harvard Medical School for imaging equipment and software; Piero Carninci and Yoshihide Hayashizaki for generating the normalized library; Frank McKeon for discussions, advice, and the anti-BubR1 antibody; Tim Yen for his gift of CENP-E antibody; Michael Rape for his generous help with somatic cell extracts; Olaf Stemmann for performing the separase assay; Scott Rodig and Frank McKeon for the NBubR1-expressing cells; Jennifer "Jake" DeLuca and Ted Salmon for anti-Hec1 antibodies; Danny Ooi for recombinant cdh1; members of the Mitchison lab for discussions; and the anonymous reviewers for helpful suggestions. A.S. is a postdoctoral fellow of the Damon Runyon Cancer Research Fund.

Received: March 9, 2004
Revised: July 12, 2004
Accepted: July 16, 2004
Published: September 2, 2004

References

Buonomo, S.B., Clyne, R.K., Fuchs, J., Loidl, J., Uhlmann, F., and Nasmyth, K. (2000). Disjunction of homologous chromosomes in meiosis I depends on proteolytic cleavage of the meiotic cohesin Rec8 by separin. Cell *103*, 387–398.

Carninci, P., Shibata, Y., Hayatsu, N., Sugahara, Y., Shibata, K., Itoh, M., Konno, H., Okazaki, Y., Muramatsu, M., and Hayashizaki, Y. (2000). Normalization and subtraction of cap-trapper-selected cDNAs to prepare full-length cDNA libraries for rapid discovery of new genes. Genome Res. *10*, 1617–1630.

Cleveland, D.W., Mao, Y., and Sullivan, K.F. (2003). Centromeres and kinetochores: from epigenetics to mitotic checkpoint signaling. Cell *112*, 407–421.

DeLuca, J.G., Moree, B., Hickey, J.M., Kilmartin, J.V., and Salmon, E.D. (2002). hNuf2 inhibition blocks stable kinetochore-microtubule attachment and induces mitotic cell death in HeLa cells. J. Cell Biol. *159*, 549–555.

Ditchfield, C., Johnson, V.L., Tighe, A., Ellston, R., Haworth, C., Johnson, T., Mortlock, A., Keen, N., and Taylor, S.S. (2003). Aurora B couples chromosome alignment with anaphase by targeting BubR1, Mad2, and Cenp-E to kinetochores. J. Cell Biol. *161*, 267–280.

Elbashir, S.M., Harborth, J., Lendeckel, W., Yalcin, A., Weber, K., and Tuschl, T. (2001). Duplexes of 21-nucleotide RNAs mediate RNA interference in cultured mammalian cells. Nature *411*, 494–498.

Funabiki, H., and Murray, A.W. (2000). The Xenopus chromokinesin Xkid is essential for metaphase chromosome alignment and must be degraded to allow anaphase chromosome movement. Cell *102*, 411–424.

Gruss, O.J., Carazo-Salas, R.E., Schatz, C.A., Guarguaglini, G., Kast, J., Wilm, M., Le Bot, N., Vernos, I., Karsenti, E., and Mattaj, I.W. (2001). Ran induces spindle assembly by reversing the inhibitory effect of importin alpha on TPX2 activity. Cell *104*, 83–93.

Hauf, S., Waizenegger, I.C., and Peters, J.M. (2001). Cohesin cleavage by Separase required for anaphase and cytokinesis in human cells. Science *293*, 1320–1323.

Hauf, S., Cole, R.W., LaTerra, S., Zimmer, C., Schnapp, G., Walter, R., Heckel, A., van Meel, J., Rieder, C.L., and Peters, J.M. (2003). The small molecule Hesperadin reveals a role for Aurora B in correcting kinetochore-microtubule attachment and in maintaining the spindle assembly checkpoint. J. Cell Biol. *161*, 281–294.

Katis, V.L., Galova, M., Rabitsch, K.P., Gregan, J., and Nasmyth, K. (2004). Maintenance of cohesin at centromeres after meiosis I in budding yeast requires a kinetochore-associated protein related to MEI-S332. Curr. Biol. *14*, 560–572.

Kerrebrock, A.W., Moore, D.P., Wu, J.S., and Orr-Weaver, T.L. (1995). Mei-S332, a Drosophila protein required for sister-chromatid cohesion, can localize to meiotic centromere regions. Cell *83*, 247–256.

Kitajima, T.S., Kawashima, S.A., and Watanabe, Y. (2004). The conserved kinetochore protein shugoshin protects centromeric cohesion during meiosis. Nature *427*, 510–517.

Li, X., and Nicklas, R.B. (1995). Mitotic forces control a cell-cycle checkpoint. Nature *373*, 630–632.

Marston, A.L., Tham, W.H., Shah, H., and Amon, A. (2004). A genome-wide screen identifies genes required for centromeric cohesion. Science *303*, 1367–1370.

Martin-Lluesma, S., Stucke, V.M., and Nigg, E.A. (2002). Role of Hec1 in spindle checkpoint signaling and kinetochore recruitment of Mad1/Mad2. Science *297*, 2267–2270.

McCleland, M.L., Gardner, R.D., Kallio, M.J., Daum, J.R., Gorbsky, G.J., Burke, D.J., and Stukenberg, P.T. (2003). The highly conserved Ndc80 complex is required for kinetochore assembly, chromosome congression, and spindle checkpoint activity. Genes Dev. *17*, 101–114.

McEwen, B.F., Hsieh, C.H., Mattheyses, A.L., and Rieder, C.L. (1998). A new look at kinetochore structure in vertebrate somatic cells using high-pressure freezing and freeze substitution. Chromosoma *107*, 366–375.

Mitchison, T.J. (1989). Polewards microtubule flux in the mitotic spindle: evidence from photoactivation of fluorescence. J. Cell Biol. *109*, 637–652.

Moore, D.P., Page, A.W., Tang, T.T., Kerrebrock, A.W., and Orr-Weaver, T.L. (1998). The cohesion protein MEI-S332 localizes to condensed meiotic and mitotic centromeres until sister chromatids separate. J. Cell Biol. *140*, 1003–1012.

Nachury, M.V., Maresca, T.J., Salmon, W.C., Waterman-Storer, C.M., Heald, R., and Weis, K. (2001). Importin beta is a mitotic target of the small GTPase Ran in spindle assembly. Cell *104*, 95–106.

Patterson, G.H., and Lippincott-Schwartz, J. (2002). A photoactivatable GFP for selective photolabeling of proteins and cells. Science *297*, 1873–1877.

Peters, J.M. (2002). The anaphase-promoting complex: proteolysis in mitosis and beyond. Mol. Cell *9*, 931–943.

Rabitsch, K.P., Gregan, J., Schleiffer, A., Javerzat, J.P., Eisenhaber, F., and Nasmyth, K. (2004). Two fission yeast homologs of Drosophila Mei-S332 are required for chromosome segregation during meiosis I and II. Curr. Biol. *14*, 287–301.

Rattner, J.B., Rao, A., Fritzler, M.J., Valencia, D.W., and Yen, T.J. (1993). CENP-F is a.ca 400 kDa kinetochore protein that exhibits a cell-cycle dependent localization. Cell Motil. Cytoskeleton *26*, 214–226.

Rieder, C.L., and Cole, R. (1999). Chromatid cohesion during mitosis: lessons from meiosis. J. Cell Sci. *112*, 2607–2613.

Salic, A., Lee, E., Mayer, L., and Kirschner, M.W. (2000). Control of beta-catenin stability: reconstitution of the cytoplasmic steps of the wnt pathway in Xenopus egg extracts. Mol. Cell *5*, 523–532.

Scanlan, M.J., Gout, I., Gordon, C.M., Williamson, B., Stockert, E., Gure, A.O., Jager, D., Chen, Y.T., Mackay, A., O'Hare, M.J., and Old, L.J. (2001). Humoral immunity to human breast cancer: antigen definition and quantitative analysis of mRNA expression. Cancer Immun. *1*, 4.

Skibbens, R.V., Skeen, V.P., and Salmon, E.D. (1993). Directional instability of kinetochore motility during chromosome congression and segregation in mitotic newt lung cells: a push-pull mechanism. J. Cell Biol. *122*, 859–875.

Sumara, I., Vorlaufer, E., Stukenberg, P.T., Kelm, O., Redemann, N., Nigg, E.A., and Peters, J.M. (2002). The dissociation of cohesin from chromosomes in prophase is regulated by Polo-like kinase. Mol. Cell *9*, 515–525.

Taylor, S.S., and McKeon, F. (1997). Kinetochore localization of murine Bub1 is required for normal mitotic timing and checkpoint response to spindle damage. Cell *89*, 727–735.

Uhlmann, F., Wernic, D., Poupart, M.A., Koonin, E.V., and Nasmyth, K. (2000). Cleavage of cohesin by the CD clan protease separin triggers anaphase in yeast. Cell *103*, 375–386.

Vagnarelli, P., Morrison, C., Dodson, H., Sonoda, E., Takeda, S., and Earnshaw, W.C. (2004). Analysis of Scc1-deficient cells defines a key metaphase role of vertebrate cohesin in linking sister kinetochores. EMBO Rep. *5*, 1–5.

Waters, J.C., Skibbens, R.V., and Salmon, E.D. (1996). Oscillating mitotic newt lung cell kinetochores are, on average, under tension and rarely push. J. Cell Sci. *109*, 2823–2831.

Waters, J.C., Chen, R.H., Murray, A.W., Gorbsky, G.J., Salmon, E.D., and Nicklas, R.B. (1999). Mad2 binding by phosphorylated kinetochores links error detection and checkpoint action in mitosis. Curr. Biol. *9*, 649–652.

Yao, X., Abrieu, A., Zheng, Y., Sullivan, K.F., and Cleveland, D.W. (2000). CENP-E forms a link between attachment of spindle microtubules to kinetochores and the mitotic checkpoint. Nat. Cell Biol. *2*, 484–491.

Zhai, Y., Kronebusch, P.J., and Borisy, G.G. (1995). Kinetochore microtubule dynamics and the metaphase-anaphase transition. J. Cell Biol. *131*, 721–734.